Distinct Stages of Stimulated FcεRI Receptor Clustering and Immobilization Are Identified through Superresolution Imaging

Sarah A. Shelby,[†] David Holowka,[†] Barbara Baird,[†] and Sarah L. Veatch[‡]*

[†]Department of Chemistry and Chemical Biology, and Field of Biophysics, Cornell University, Ithaca, New York; and [‡]Department of Biophysics, University of Michigan, Ann Arbor, Michigan

SUPPORTING MATERIALS

SUPPORTING RESULTS

Live RBL-2H3 cells retain antigen-stimulated degranulation and Ca^{2+} responses under super-resolution imaging conditions.

To determine whether the buffer conditions required for dSTORM imaging affect the functional responses which result from IgE receptor cross-linking, a β-hexosaminidase release assay was used to measure the levels of secretory granule release in adherent RBL-2H3 cells in response to antigen stimulation conditions similar to those used in our live cell super-resolution experiments. This assay utilizes a fluorogenic substrate for the enzyme β-hexosaminidase, a constituent of secretory granules, to measure its release as a consequence of degranulation and quantify the extent of degranulation in RBL-2H3 cells (1). Control samples were stimulated under conditions that are conducive to degranulation in balanced salt solution with 1 mg/ml BSA (BSS-BSA, 30mM HEPES, 135mM NaCl, 5mM KCl, 1mM $MgCl_2$, 1.8mM $CaCl_2$, 5mM glucose, and 1mg/ml BSA at pH 7.4) at 37°C. Our super-resolution imaging buffer is buffered with Tris and has a higher pH than BSS (pH 8), contains the reducing agents and oxygen scavenging enzymes necessary for dSTORM imaging of AlexaFluor 647, and also has a higher concentration of glucose (55mM), which is a substrate for the oxygen-scavenging enzyme glucose oxidase. To determine the effects of the various components of the imaging buffer on cellular degranulation, cells were stimulated in imaging buffer with or without 50mM of glutathione (GTT) and oxygen scavenging enzymes. These cells degranulate to a slightly lesser extent than cells stimulated in BSS-BSA (Fig. S1 *A*), although degranulation is still robust. Degranulation in the presence of this buffer is reduced to levels between 75 and 90% of degranulation measured in BSS-BSA according to data shown in Fig. S1 and Fig. S8. Cellular degranulation measured in cells in imaging buffer without a reducing agent or oxygen scavenging enzymes is not significantly different from degranulation of cells in imaging buffer that contains both 50mM glutathione and oxygen scavenging enzymes. The decreased degranulation of cells in imaging buffer that contains both 50mM glutathione and oxygen scavenging enzymes compared to cells in BSS-BSA appears to be due to other components of the imaging buffer that differ from BSS-BSA, possibly the increased glucose concentration, Tris buffer, or increased pH. Stimulated cellular degranulation is substantially less when a higher concentration of glutathione is used or when β-mercaptoethanol is used as the imaging buffer reducing agent. For this reason a 50mM glutathione was chosen to minimize the impact of imaging buffer conditions on cellular responses, and the final formulation of the imaging buffer (IB) contains 30mM Tris, 135mM NaCl, 5mM KCl, 1mM $MgCl_2$, 1.8mM $CaCl_2$, 55mM glucose, 500μg/mL glucose-oxidase, 40μg/mL catalase, and 50mM glutathione at pH 8.

The effect of imaging buffer on Ca^{2+} mobilization was assessed through imaging experiments where sensitized RBL-2H3 cells are loaded with the Ca^{2+}-sensitive dye Fluo-4 and stimulated with multivalent antigen (DNP-BSA) in the presence of imaging buffer at room temperature (Fig. S1, *A* and *B*). Fluorescence intensity is monitored across a field of several hundred cells as a function of stimulation time, as described in Materials and Methods. Cells produce a robust Ca^{2+} response in the presence of imaging buffer after stimulation by antigen compared to cells imaged and stimulated in the conventional live cell imaging buffer, BSS-BSA (Fig. S1 *B*). The cumulative distribution of cells with an initial Ca^{2+}response indicates that the onset of Ca^{2+} mobilization in the population of cells is not substantially delayed or otherwise affected by imaging buffer (Fig. S1 *C*).

Redistribution of IgE-FcεRI after antigen addition as imaged in chemically fixed cells.

Super-resolution fluorescence localization imaging of IgE-FcεRI at the ventral (bottom) surface of chemically fixed RBL-2H3 cells reveals time-dependent receptor clustering due to cross-linking by antigen (Fig. S2), in good agreement with previous electron microscopy studies (2). Cells were sensitized by incubating with IgE antibodies specific for DNP, stimulated with the multivalent antigen DNP-BSA, and then chemically fixed at specified time points after antigen addition, as described in Materials and Methods. IgE-FcεRI complexes were fluorescently labeled either by sensitizing with IgE directly conjugated to Alexa Fluor 647 (AF647) (Fig. S2 *A* and *B*), or by sensitizing cells with two distinct pools of IgE directly conjugated either to AF647 or to Alexa Fluor 532 (AF532) prior to antigen addition and fixation (Fig. S2 *C*). Conventional TIRF images of the single-color fixed cells (Fig. S2 *A*) were captured before single-color super-resolution images (Fig. S2 *B*) and are shown for comparison. For super-resolution images with both single- and two-color labeling, IgE-FcεRI appears weakly structured in unstimulated cells (-Ag) and exhibits a clustered appearance in cells after stimulation (+Ag). One minute after antigen addition, labeled IgE-FcεRI-rich patches become apparent around the periphery of the cell's ventral surface, likely because this is the area accessed first by antigen. After incubation with antigen for 5 or 10 min, cells contain distinct IgE-FcεRI puncta on the ventral cell surface. Conventional TIRF imaging also shows large-scale receptor organization, including receptor puncta in stimulated cells, but structures under ~250nm cannot be resolved.

As with live cell experiments, we utilize spatial pair correlation functions to quantify clustering of IgE-FcεRI complexes in single-color reconstructed images of fixed cells. In single color experiments, multiple AF647 fluorophores can label each IgE antibody and each AF647 fluorophore can reversibly transition between fluorescent and non-fluorescent states within a single experiment. These phenomena result in apparent clustering on the size-scale of the localization precision in super-resolution images, such as those shown in Fig. S2 *B*, and corresponding artifacts in the quantification of images due to over-counting of single receptors (3). Pair cross-correlation functions are not subject to over-counting artifacts(3), are tabulated from two-color images, and measure the normalized probability of finding a localized fluorophore of one color a given distance, r, away from the average localized fluorophore of the second color. Average cross-correlation functions tabulated from unstimulated and stimulated cells are shown in Fig. S2 *D*.

Measured cross-correlation functions are fit to a single filtered exponential to extract information on average cluster size and density (3):

$$g_{Fit}(r) = g_{PSF}(r)*[1+ (Aexp(-r/\xi))]. \quad (S\ 1)$$

A is the amplitude of correlations, which is related to the increased density of receptors in clusters, ξ is the correlation length, which is approximately the average cluster radius, and $g_{PSF}(r)$ is a function that applies a Gaussian filter with width proportional to the resolution of the image. Measured cross-correlation functions were fit for all radii r<500nm. Details of the fitting methods and the determination of the resolution of the image are described in Materials and Methods. Simulated receptor density distributions which are reconstructed from our observed cross-correlation functions are shown in the right panels of Fig. S2 *D* and serve as a visual aid to represent receptor distributions in the absence of over-counting. We also fit autocorrelation functions tabulated from single color images to Eqn. S1 after first subtracting expected contributions from over-counting, assuming an average surface density of IgE-FcεRI complexes of 200/μm^2 (3, 4). Summaries of extracted values for ξ and A from both single and two color images are shown in Fig. S2 *E* and F along with our past results applying a similar analytical

methodology to scanning electron microscopy (SEM) images of IgE-FcεRI on the dorsal surface of RBL-2H3 cells labeled post fixation with primary and gold-conjugated secondary antibodies (2).

In unstimulated cells (-Ag), the cross-correlation of AF647 and AF532 probes is close to one at all radii, indicating that IgE-FcεRI complexes are nearly randomly distributed on the membrane (Fig. S2 *D*). Upon closer inspection, cross-correlation functions tabulated from images of cells indicate the presence of weak, long-range correlations in cells in the absence of antigen (inset of Fig. S2 *D*). The size of correlations in unstimulated cells is comparable to the size of clusters at long stimulation times, but the amplitude associated with these correlations is only 20% greater than a random distribution of receptors (Fig. S2 *D* inset), and two orders of magnitude less than the correlation amplitude 5 min following antigen stimulation. The simulated receptor distribution displayed in Fig. S2 *D* (lowest right panel) that corresponds to the unstimulated correlation function is a visual representation of these weak correlations and is nearly indistinguishable from a random distribution. We previously proposed that weak, long-range, unstimulated clustering may arise from non-planar topology of the ventral membrane, from weak lipid-mediated organization in unstimulated cells (3), or through direct or indirect coupling to cortical actin (5, 6). We note that no equivalent correlations were observed in our previous SEM work in unstimulated cells, which selected for flat regions of the dorsal cell surface (2). Also, weak correlations are dominated by over-counting artifacts in autocorrelation functions tabulated from unstimulated cells labeled with a single color. Errors in the estimation of correlations from over-counting likely result in an underestimation of ξ and an over-estimation of A for single-color measurements.

Cross-correlation functions become larger than one at short radii in cells incubated with multivalent antigen prior to fixation, indicating that receptors become clustered. With increasing stimulation time, cross-correlations increase in magnitude at short radii. Cross-correlation functions, calculated from images of stimulated cells, remain larger than one out to radii of 200 nm, indicating that the largest clusters have approximately this radius. This quantitative treatment is consistent with the qualitative observation of clustering in representative images shown in Fig. S2, *B* and *C*. Variations in the size (ξ) and magnitude (A) of correlations as a function of stimulation time provide a quantitative measure of receptor redistribution with cross-linking. We observe a slight increase in the size of cross-linked receptor clusters (ξ) within 5 min after stimulation, similar to the modest increase we observe in live cells after stimulation (Fig. 1C).Values of ξ are in relatively good agreement with our past SEM data, which, like our single-color experiments, are corrected for over-counting (Fig. S2 *E*) (2). Observed differences between the dorsal cell surface imaged by SEM and the ventral cell surface imaged by super-resolution microscopy, could arise from different accessibility to antigen or differences arising from adhesion to the substrate.

The amplitude of correlations (A) also increases with stimulation time, corresponding to an increase in receptor density in clusters (Fig. S2 *F*). It is notable that the correlation amplitude is substantially larger in stimulated cells in super-resolution measurements when compared to our previous SEM studies (Fig. S2 *F*). This indicates that clustered fluorescent labels in these optical microscopy measurements are more densely packed than the gold particles observed by SEM. This could be accounted for if gold particles are precluded from labeling some IgE-FcεRI complexes in densely packed receptor clusters due to the large relative size of the primary and secondary antibodies and gold particles (10 nm diameter). Values of ξ and A extracted from single color and two color images are in good general agreement aside from systematic reductions in ξ and elevation in A for single-color data.

Again, these systematic errors are expected with underestimation of correlations due to over-counting in the single color measurements, since remaining contributions from over-counting would act to decrease ξ and increase A.

Cholesterol perturbations affect antigen-stimulated degranulation and Ca^{2+} responses in live cells.

To probe the effects of cholesterol perturbations on signaling downstream of initial receptor clustering, we observed the Ca^{2+} responses of cells subjected to cholesterol depletion using methyl-beta-cyclodextrin (MβCD) or cholesterol enrichment using MβCD -cholesterol (MβCD+chol) similar to conditions used for live cell super-resolution experiments. Cytoplasmic Ca^{2+} concentrations were imaged using the Ca^{2+}-sensitive dye Fluo-4 for large fields of cells treated with MβCD or MβCD+chol (or neither in the case of control cells) followed by stimulation with antigen as described in the Materials and Methods and shown in Fig. 6. We observe perturbation-dependent differences in the shape, duration, and frequency of oscillations in the Fluo-4 intensity traces for individual cells (Fig. S7). Compared to untreated cells, Ca^{2+} oscillations due to the addition of antigen are delayed in individual MβCD-treated cells, and oscillations are less frequent (Fig.S7, top), consistent with the attenuated total intensity and delayed onset of initial Ca^{2+} responses we observe for the population of cells (Fig. 6, *B* and *C*). MβCD+chol treated cells begin to display Ca^{2+} oscillations upon the addition of MβCD+chol. These oscillations are robust for ~2 min but decrease in amplitude quickly after that time. Upon antigen addition, MβCD+chol-treated cells exhibit solitary, low-amplitude increases in cytoplasmic Ca^{2+} but do not display regular oscillations as in the case of untreated cells.

The β-hexosaminidase release assay was used to measure the levels of degranulation in adherent RBL-2H3 cells in response to cholesterol perturbation and antigen stimulation conditions similar to those used in our live cell cholesterol perturbation super-resolution experiments (Fig. 6). Cholesterol reduction results in a slight increase in spontaneous degranulation in the absence of antigen and a decrease in antigen-stimulated degranulation compared to cells in the presence or absence of antigen which are not subjected to cholesterol perturbation (Fig. S8). Similar experiments have previously been reported in the literature and have shown mixed results for the effect of cholesterol reduction on degranulation, where some report enhanced degranulation without stimulation and/or inhibited degranulation in the presence of antigen, and others do not observe significant changes (7–11). However, these previous experiments were conducted under varying conditions of cholesterol reduction, stimulation, etc, which may have significant effects on degranulation measurements. Cholesterol enrichment strongly inhibits degranulation either in the presence or absence of antigen. This suggests that although we observe clustering in super-resolution experiments and transient increases in cytoplasmic Ca^{2+} upon treatment of cells with MβCD+chol, these responses to cholesterol loading do not result in signaling sufficient for degranulation.

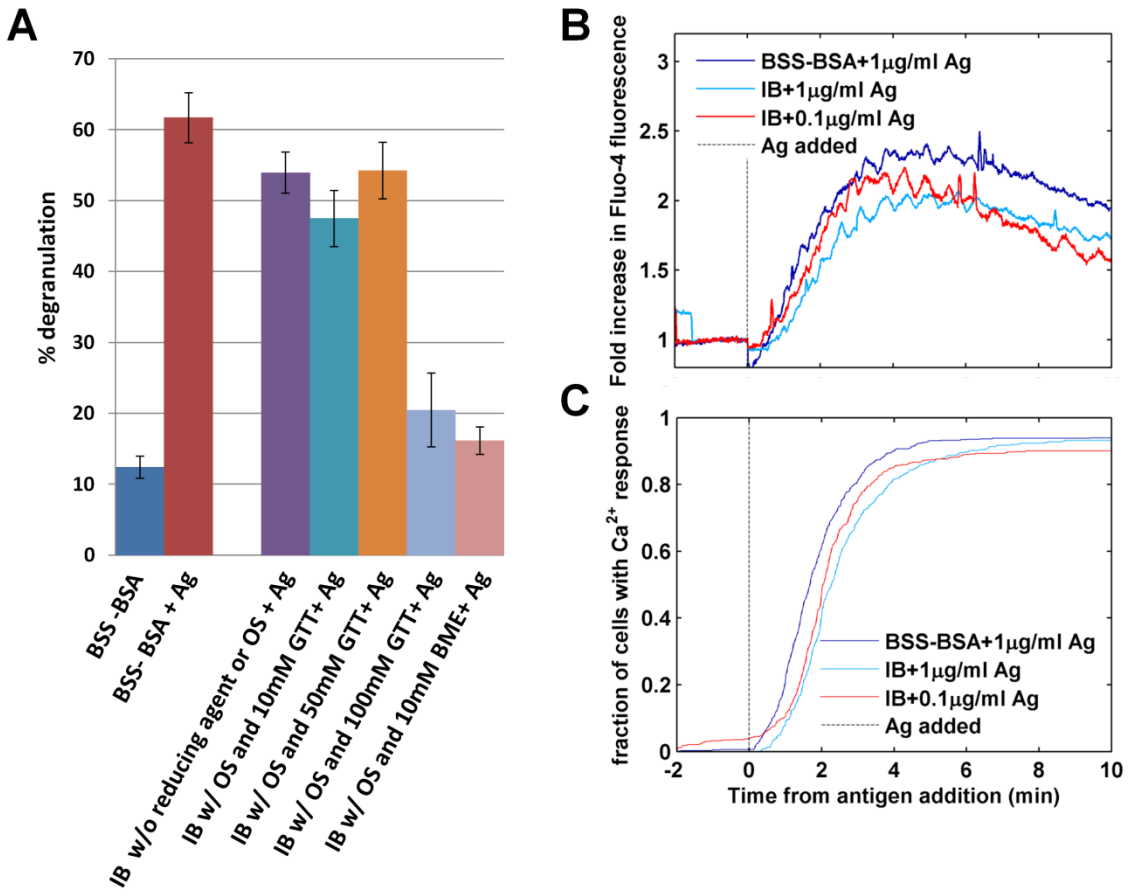

Fig. S1: RBL-2H3 cells retain the antigen-stimulated responses in super-resolution imaging buffer. (A) RBL-2H3 degranulation at 37°C was measured using a β-hexosaminidase release fluorogenic assay in which the effects of the oxygen scavenging enzymes (OS) and reducing agent used in the dSTORM imaging buffer (IB), including glutathione (GTT) or beta-mercaptoethanol (BME), were tested on antigen-stimulated degranulation. Cells in BSS-BSA in the presence or absence of DNP-BSA (1 μg/ml) were used as standards for basal and stimulated degranulation, respectively. (B) Antigen-stimulated Ca^{2+}mobilization was measured in the presence of imaging buffer at room temperature using Fluo-4 intensity as a readout of intracellular Ca^{2+} concentration. Total fluorescence intensity is shown for populations of cells (at least 500) loaded with Fluo-4-AM and stimulated with 1μg/ml or 0.1 μg/ml multivalent antigen (DNP_{24}-BSA) in BSS-BSA or in the presence of super-resolution imaging buffer as a function of time. The dotted gray line at 0 min indicates the addition of antigen. The signal is normalized to initial levels, and intensity is reported as a fold increase from initial levels. (C) Cumulative curves of Ca^{2+} mobilization initiation events of individual cells as a function of time. The number of cells which have initiated a Ca^{2+} response is plotted as the fraction of the total number of cells which displayed a Ca^{2+} response during the experiment.

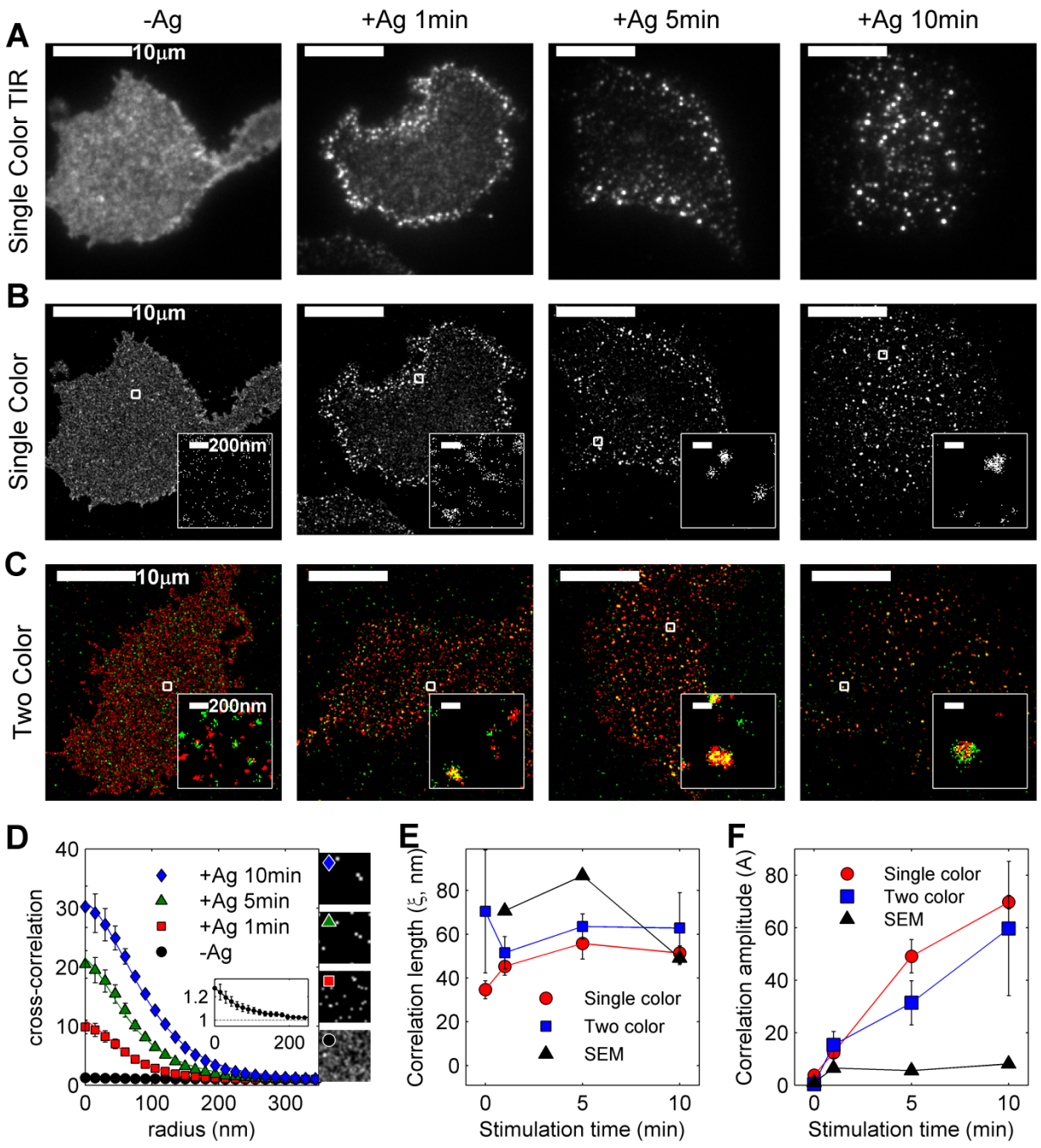

Fig. S2: Quantitative super-resolution localization microscopy TIRF imaging of IgE-FcεRI redistribution after antigen addition in chemically fixed cells. Representative TIRF images of RBL-2H3 cells imaged using either (A)conventional TIRF microscopy, (B) single-color, or (C) two-color super-resolution fluorescence localization microscopy in unstimulated cells and cells treated with the multivalent antigen DNP-BSA (1 μg/ml) at 37°C for the time indicated before chemical fixation. Conventional TIRF and single color super-resolution images are shown for the same 4 cells in (A) and (B), respectively, for purposes of comparison between super-resolution and conventional images. Single-color cells in (A) and

(B) are sensitized with IgE directly conjugated to AF647, while two-color measurements in (C) were conducted on cells sensitized with IgE directly conjugated to either AF647 (red) or AF532 (green) fluorophores. (D) Cross-correlation curves evaluated from two-color measurements averaged over at least 5 cells for each stimulation condition shown in (C). Error bars represent the standard error of the mean of values between cells. Lines are a fit to Eqn. S1 for radii between 0 and 500nm. Simulated receptor distributions over a 2μm by 2μm area which recapitulate observed correlation functions for each time point are shown at right. Extracted correlation lengths (E) and amplitudes (F) from super-resolution fluorescence localization imaging measurements are compared to previous scanning electron microscopy (SEM) measurements (2). Values reported for two-color measurements represent the average over multiple cells with error bounds denoting the standard error of the mean. For single-color measurements, values are obtained by correcting measured correlation functions for over-counting assuming a receptor density of 200/μm^2, and fitting the resulting curve to Eqn. S1 for radii between 40 and 300nm.

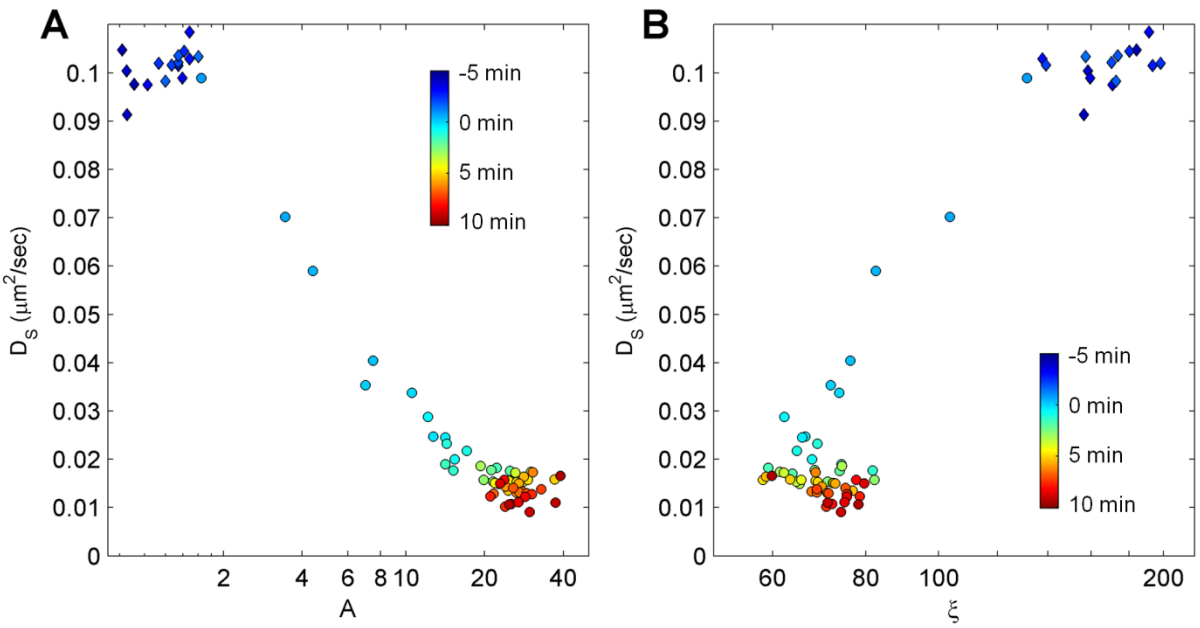

Fig. S3: Average receptor diffusion vs. correlation amplitude and correlation length. Average short time diffusion coefficient (as in Fig. 2 *C*) is shown as a function of the correlation function parameters, the correlation amplitude A (A) and the correlation length ξ (B) (as in Fig. 1 *C*). Each point corresponds to values of D_s and A or ξ at a given time before (diamonds) and after (circles) stimulation averaged over the 11 cells imaged, and data from individual cells are binned every 15 s to facilitate averaging. These plots are related to Fig. 3 A because the parameters N, A, and ξ are not independent. If correlation functions are well approximated by exponentials, then $N \approx 2A\xi^2\rho$, where ρ is the average receptor density which is assumed to be 200/μm^2 (4). In Fig. 3 A, N is determined without fitting according to Eqn. 2. Time after the addition of antigen is indicated by the color bar. Antigen (1 μg/ml) is added at time = 0, after the cells were imaged for 5 min.

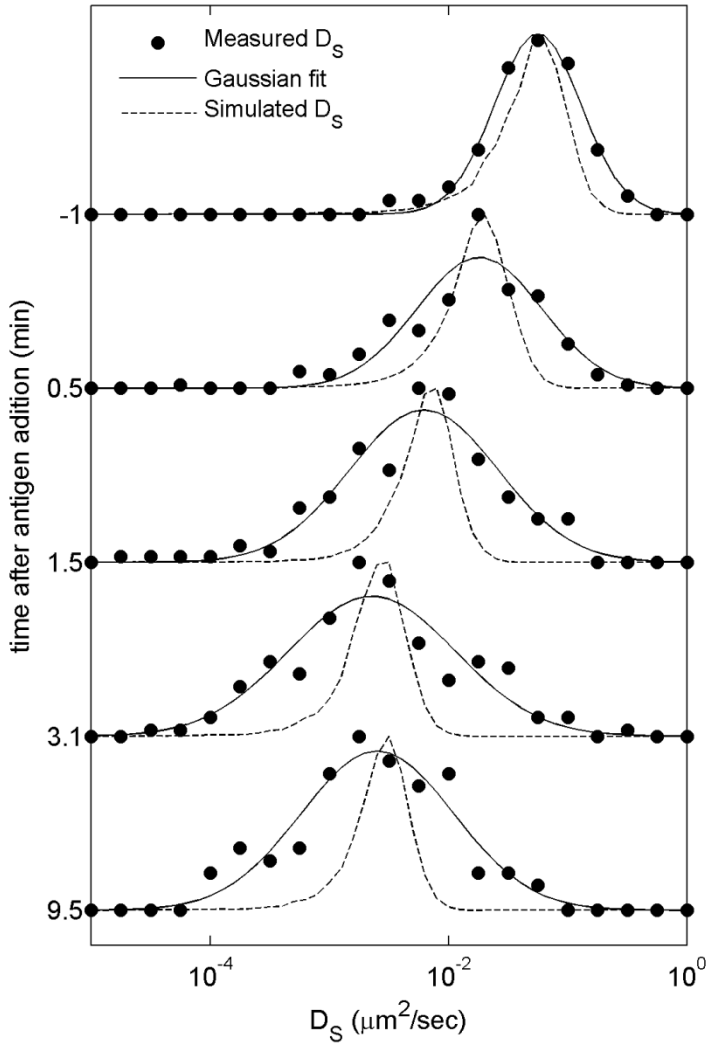

Fig. S4: Distributions of single-trajectory diffusion constant are broader than expected for Brownian diffusion post-stimulation. Histograms showing the distribution of single molecule diffusion coefficients (D_S) are repeated from Fig. 4 *B* (solid points) and compared with histograms generated by extracting D_S from simulated Brownian trajectories with the same distribution of track lengths observed in experiments (dashed lines). The width and asymmetric shape of simulated histogram arises from their being finite track lengths (at least 16 segments). Before the addition of antigen (top), the widths of diffusion coefficient histograms are well approximated by the Brownian simulation, suggesting a homogenous population of receptors is resolved in these measurements. After stimulation, measured histograms shift to lower values of D_S, and broaden when compared to the Brownian simulations.

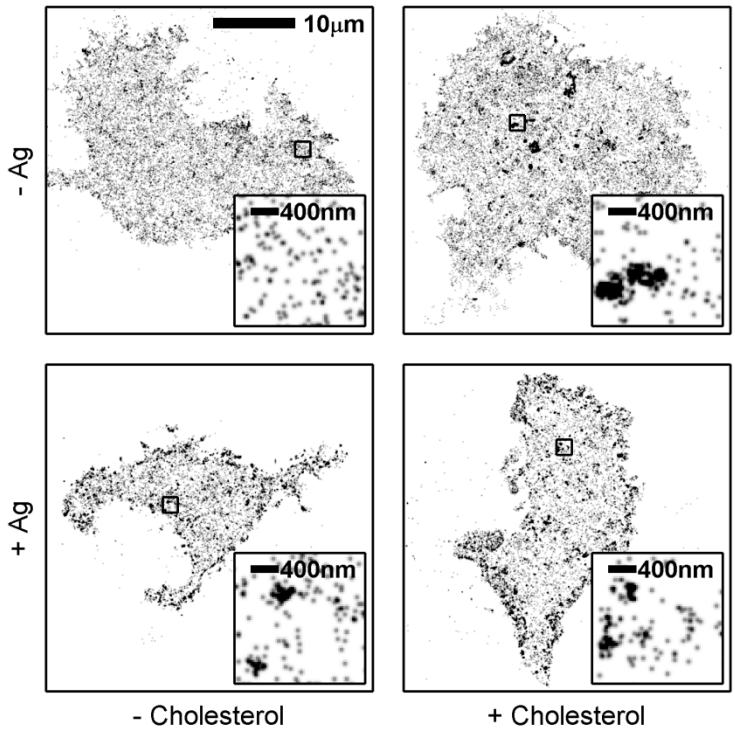

Fig. S5: Perturbations of membrane cholesterol alter receptor clustering. Representative images of live cells after 15 min of 10mM MβCD (left) or MβCD+chol(right) in the absence (top) or presence (bottom) of incubation with 0.1 μg/ml antigen for 10 min. Images are reconstructed from 80 s of acquired data. Insets show magnified images of the regions outlined with black squares.

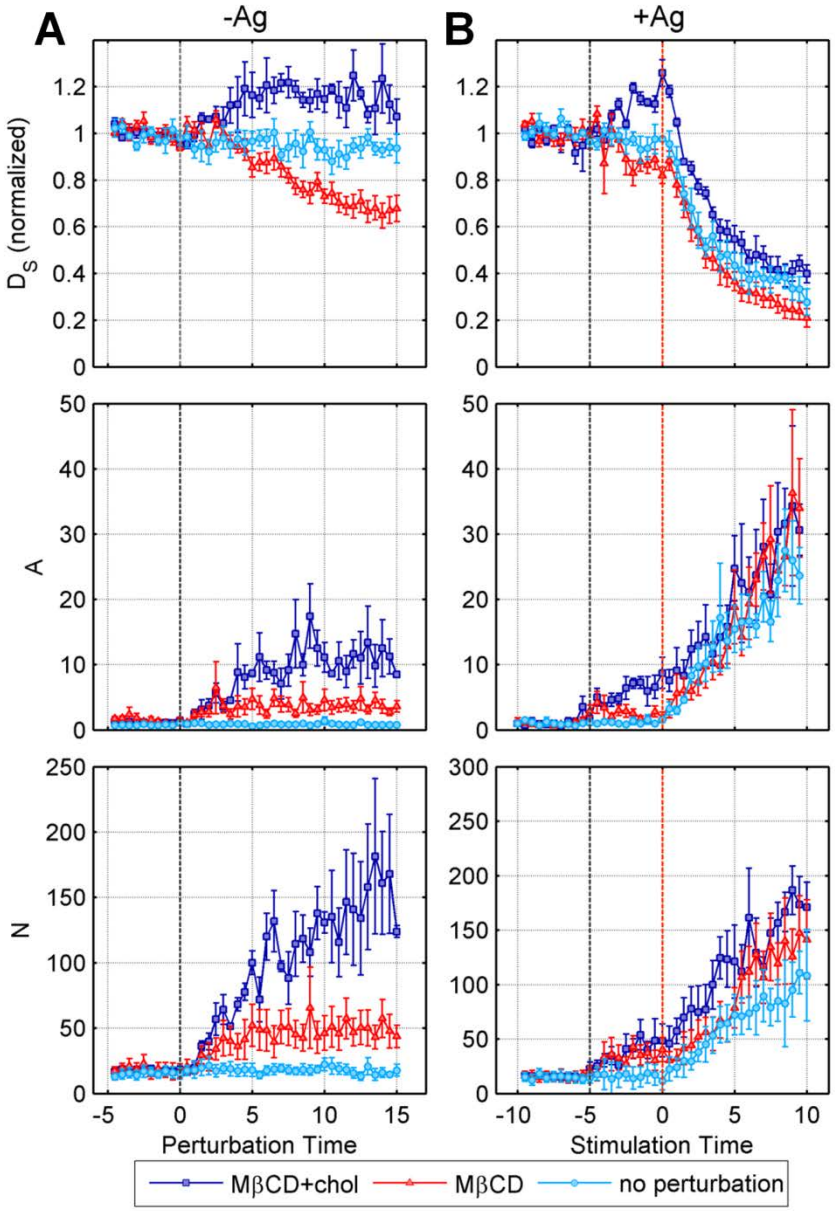

Fig. S6: Cholesterol perturbation affects average parameter values in live cell experiments. The effects of methyl-β-cyclodextrin (MβCD, red) and cholesterol-complexed methyl-β-cyclodextrin (MβCD+chol, dark blue) on average values for AF647-IgE short-time diffusion constant D_S, correlation function amplitude (A), and average number of correlated proteins (N) are measured as a function of time after the addition of the perturbation (gray dashed line). These are compared to control experiments where no perturbation is added (light blue). In (A), cells are treated with MβCD or MβCD+chol alone (or no treatment for control cells), and in (B), cells are stimulated with antigen 5 min after MβCD or MβCD+chol is added (orange dashed line), or 10 min after the start of imaging for control cells. In (A) and (B), each time trace represents the average of 4-5 independent live cell experiments. Error bars represent standard error of the mean.

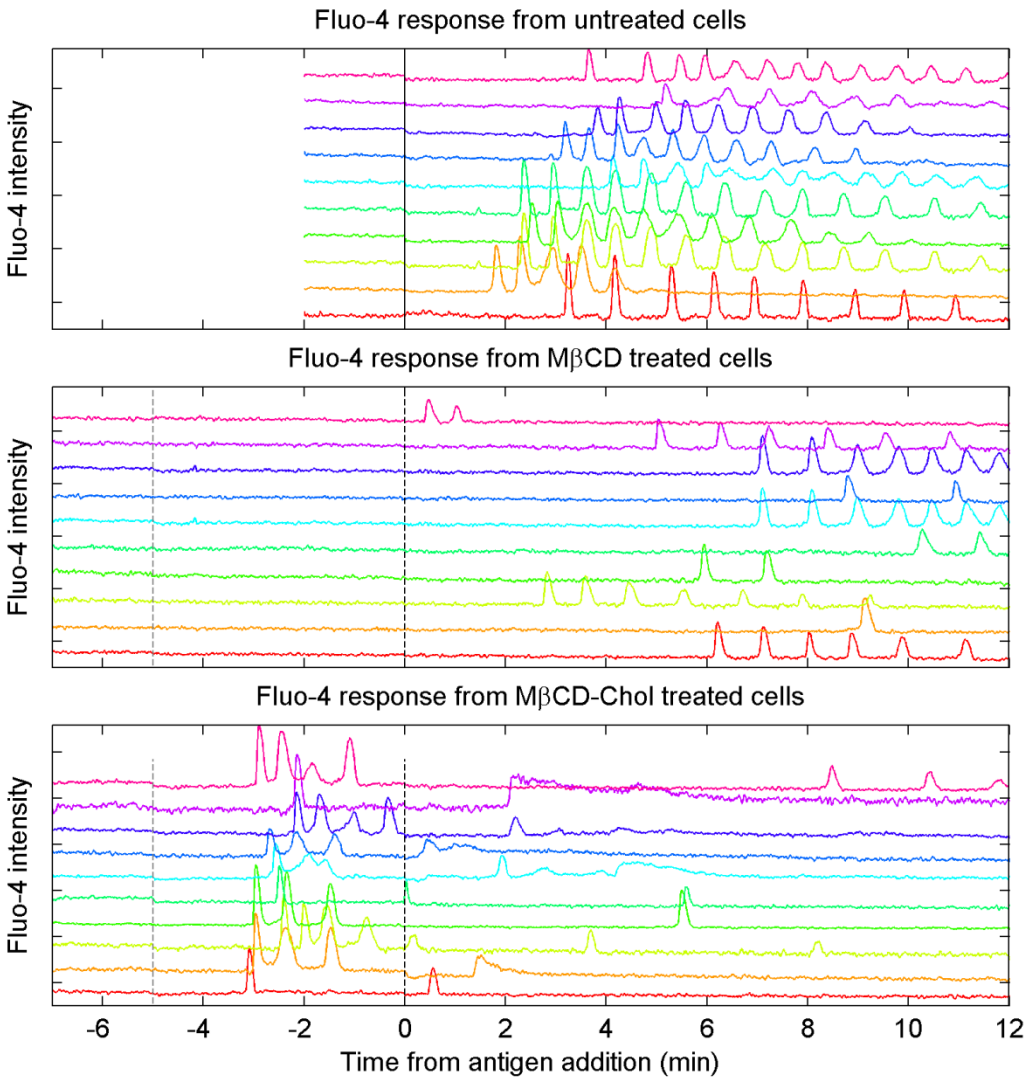

Fig. S7: The shape, frequency, and duration of Ca^{2+} oscillations are severely affected by changes in cellular cholesterol. Cytoplasmic Ca^{2+} concentrations were imaged for large fields of Fluo-4-AM loaded cells treated with MβCD (top), MβCD+chol (bottom), or neither in the case of control cells (middle), followed by stimulation with antigen as described in the Materials and Methods. Fluo-4 intensity traces are shown for representative individual cells, where intensity traces are displaced on the y axis and the y axis also delineates Fluo-4 intensity for individual cells. Traces are shown in different colors for clarity. The dotted gray line at -5 min indicates the addition of MβCD or MβCD+chol, and the dotted black line indicates the addition of 0.1µg/ml DNP-BSA.

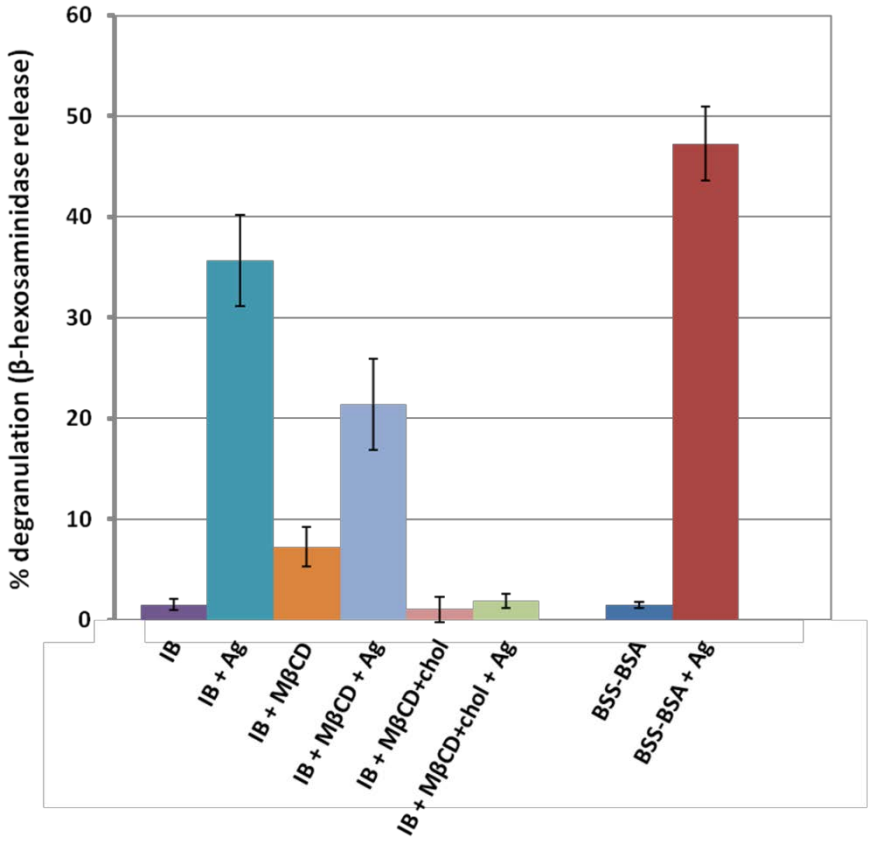

Fig. S8: Cholesterol perturbations affect the extent of antigen-stimulated degranulation as measured by β-hexosaminidase release. RBL-2H3 degranulation was measured using a β-hexosaminidase release fluorogenic assay in super-resolution imaging buffer (IB) at 37°C, with and without addition of 0.1 µg/ml DNP-BSA (Ag), and in the presence or absence of 10mM MβCD or MβCD+chol. β-hexosaminidase signal has been normalized using samples of cells lysed with TritonX-100 (TX-100) as a measure of total β-hexosaminidase content. Error bars represent standard error of the mean of multiple samples measured for each condition. Additional control samples were made in BSS + 1mg/ml BSA to test for the effect of the imaging buffer.

MATERIALS AND METHODS

Chemicals and Reagents

Amine reactive AlexaFluors 647 and 532 (AF647 and AF532), Fluo-4-AM, and Tetraspeck .125 μm fluorescent nanospheres were purchased from Life Technologies (Carlsbad, CA). β-mercaptoethanol, reduced L-glutathione, methyl-β-cyclodextrin, cholesterol-complexed methyl-β-cyclodextrin, glucose oxidase, and catalase were purchased from Sigma (St. Louis, MO). AF532 and AF647 -IgE were prepared by conjugating purified mouse monoclonal anti-2,4-dinitrophenyl (DNP) IgE with AF532 or AF647, as previously described (12, 13). AF647-IgE was measured to have a dye:protein ratio of 2.2:1. Multivalent antigen, dinitrophenyl- conjugated BSA (DNP-BSA), with an average of 24 DNP molecules per BSA was prepared as described previously (14). Glutaraldehyde (25% stock) was purchased from Ted Pella (Redding, CA). Para-formaldeyde was purchased from Electron Microscopy Services (Hatfield, PA). Cell culture supplies including MEM, Trypsin-EDTA, and gentamicin sulfate were purchased from (Life Technologies), and FBS was purchased from Atlanta Biologicals (Atlanta, GA). Cell culture dishes were purchased from MatTek (Ashland, MA).

Sample Preparation

Rat Basophilic Leukemia (RBL-2H3) cells were maintained with media containing MEM 20% FBS, 10 μg/ml gentamicin sulfate as described previously (12), then harvested using Trypsin-EDTA. MatTek Dishes were prepared with fiduciary markers by applying a dilute (1:1000 dilution in phosphate-buffered saline) solution of Tetraspeck fluorescent nanospheres to freshly oxygen plasma-cleaned wells for 15 minutes before rinsing three times with RBL-2H3 media. Cells were then plated sparsely in the dishes (0.1×10^6/well) overnight at 37°C.

Fixed cell samples:

The cells were sensitized with either AF647-labeled IgE (1μg/ml) (for single-color experiments) or a mixture of AF647-labeled IgE and AF532-labeled IgE (1μg/ml total) (for two-color experiments) in HEPES-buffered media (80% MEM, 20% fetal bovine serum, 50mg/L gentamicin, and 20mM HEPES) for 1 to 2 hours at room temperature. Dishes containing cells were rinsed and incubated in media at 37ºC for 5 minutes, rinsed again with warm PBS, treated with 1 μg/mL DNP-BSA in media (for 0,1,5, or 10 min) at 37°C, rinsed with warm PBS, and then chemically fixed (4% paraformaldehyde 0.1% glutaraldehyde in PBS) for 10 minutes at room temperature. Samples were then blocked with 2% fish gelatin, 2 mg/mL BSA in PBS for 10 minutes. For both single- and two-color experiments, fixed samples were washed 3 or more times with PBS and once with buffer containing 100mM Tris, 10mM NaCl, and 10% w/w glucose before imaging.

Live cell samples:

The cells were sensitized with AF647-labeled IgE (1μg/ml) in HEPES-buffered media for 1 to 2 hours at room temperature. Dishes containing sensitized cells were rinsed first with media, then once with super-resolution imaging buffer (IB: 30mM Tris, 135mM NaCl, 5mM KCl, 1mM $MgCl_2$, 1.8mM $CaCl_2$, 55mM glucose, 500μg/mL glucose-oxidase, 40μg/mL catalase, and 50mM glutathione at pH 8) before imaging.

Super Resolution Imaging

Imaging Setup:
Single label fixed samples were imaged on an inverted microscope (Leica DM-IRB, Wetzlar, Germany) under TIRF illumination through a 1.42 numerical aperture (N.A.) 100X Leica objective lens with a 100mW 642nm diode-pumped solid state (DPSS) laser (Crystalaser, Reno, NV) which is attenuated with neutral density filters as needed for the illumination requirements of the experiment. Typical laser power used during super-resolution data collection was about 60mW at the sample. Two-color experiments on fixed cells were conducted on an inverted Olympus IX81-ZDC microscope with a cellTIRF module (Olympus America, Center Valley, PA) under TIRF illumination though a 1.45 N.A. 100X Olympus objective lens with either a variable power 75mW 642nm DPSS laser (Coherent, Santa Clara, CA) or a 150mW DPSS 532 laser (Cobolt, Stockholm, Sweden). In both instrument setups, images were recorded with an Andor iXon 897 EM-CCD camera (Belfast, UK) using custom image acquisition code written in Matlab (The MathWorks, Natick, MA). Live cell samples were imaged on both microscopes. The camera field of view was cropped during imaging to include only a region of interest that encompasses the entire cell being imaged in order to reduce image file size and increase the camera frame rate. Camera frame rates were dependent on our exposure time of 10ms, camera settings, and the size of the cropped region of interest.

Fixed cell imaging:
Cells were imaged in the presence of an oxygen-scavenging and reducing imaging buffer (100mM Tris, 10mM NaCl, 10% w/w glucose, 500 μg/mL glucose-oxidase, 40μg/mL catalase, and 1% β-mercaptoethanol at pH 8.5). After individual cells were located using relatively low power illumination, laser power was increased to induce AF647, or AF532 photo-switching. Movies of AF647, or AF532 photo-switching were acquired with 10ms exposure time at frame rates between 25 and 32 frames per second for at least 2500 frames.

Live cell imaging:
Live cells were imaged at room temperature to limit the effects of receptor internalization during the imaging experiment. Imaging was performed in the presence of super-resolution imaging buffer (IB: 30mM Tris, 135mM NaCl, 5mM KCl, 1mM $MgCl_2$, 1.8mM $CaCl_2$, 55mM glucose, 500μg/mL glucose-oxidase, 40μg/mL catalase, and 50mM glutathione at pH 8). Live cells were imaged at room temperature with frame exposure times of 10ms and frame rates between 25 and 32 fps for at least 5 minutes before addition of DNP_{24}-BSA at a final concentration of 1μg/ml and monitored as stimulation progressed for at least 10 minutes for data reported in Figs. 1-4, S2, and S4. In experiments where antigen was competed off of surface IgE using DNP aminocaproyl-L-tyrosine (DCT), a stimulating dose of 0.1μg/ml antigen was used, and DCT at a final concentration of 20 μM was added 7 minutes after antigen addition (Fig. 5). Cells were imaged for at least 10 minutes after the addition of DCT. In membrane cholesterol perturbation experiments (Figs 6, S5, S6, S7, and S8), methyl-β-cyclodextrin (MβCD) or cholesterol-complexed methyl-β-cyclodextrin (MβCD+chol) was added at a final concentration of 10mM 5 min before the addition of either DNP-BSA at a final concentration of 0.1ug/ml or a blank addition of an equivalent volume of buffer in experiments where cells were not stimulated. In experiments when cholesterol perturbation is followed by stimulation with DNP-BSA, cells were imaged for an additional 5 minutes in the presence of MβCD or MβCD+chol before antigen was added at a final

concentration of 0.1ug/ml. The cells were then imaged for at least 10 minutes following stimulation. In experiments where cells were not stimulated after cholesterol perturbation, they were imaged for at least 15 minutes after addition of MβCD or MβCD+chol.

Image Analysis

Super-resolution image reconstruction:

Movies of AF647 or AF532 photoswitching were analyzed as described in (3). In brief, diffraction-limited spots are fit to a two-dimensional Gaussian function though least squares fitting using the built-in Matlab function *fminfunc()*. Localized probes that are outliers in spot width, brightness, aspect ratio, and 2D gaussian fit quality are excluded from the reconstructed image. In fixed cell measurements, probes that are localized in the same position in sequential frames, within twice the average localization precision, are combined. For live cell experiments, single molecule trajectories are determined as described below and only the first localization positions are included in reconstructed images. The average number of localizations that are accepted after culling and grouping is 12 per 10ms frame. For all experiments reconstructed images are assembled by incrementing a pixel value once for each time a localized signal is identified at that location. These images are then convolved with a two-dimensional Gaussian for display purposes. Super-resolution images are reconstructed from varying numbers of individual frames of raw data. For example, fixed cell images are reconstructed from at least 2500 frames (~100 s of integrated imaging time) of raw data, amounting to a total of approximately 30,000 single localizations, whereas live cell images are reconstructed from between 500 and 2000 frames (~20 and 80 s integrated imaging time), amounting to between approximately 6,000 and 24,000. The localization precision was calculated from correlation functions as described in (3) and had typical values around 20nm for a given imaging experiment using AF647 as the super-resolution probe.

Correlation function analysis of super-resolution images:

Receptor clustering in super-resolution images is analyzed using spatial auto- and cross-correlation functions. Correlation functions are calculated from reconstructed images of localized fluorophores as described previously (3). Briefly, reconstructed images (I) are masked (M) to exclude contributions from cell edges, and autocorrelation functions are tabulated using fast Fourier transforms (FFTs) according to:

$$g(r) = 1/ \rho^2 \times FFT^{-1}(|FFT(I)|^2)/ FFT^{-1}(|FFT(M)|^2)$$

where ρ is the average density of localized signals within the masked region. The autocorrelation of the mask is included to properly account for boundary conditions. A Matlab function that tabulates g(r) from images is included in Supplementary material in (3). Cross-correlation functions for fixed cell images are tabulated similarly from masked images from two distinct images I_1 and I_2 with average densities ρ_1 and ρ_2 according to:

$$c(r) = 1/(\rho_1 \rho_2) * RE(FFT^{-1}(FFT(I_1) \times FFT(I_2)^*)))/ FFT^{-1}(|FFT(M)|^2)$$

where * denotes a complex conjugate and RE() indicates the real part. Auto-correlation functions from single color live cell images were quantified as described in the main text.

Correcting for over-counting in fixed cell images:
Auto-correlation functions from single-color fixed cell images are subject to additional clustering due to over-counting of labeled proteins, and quantifications are corrected for possible over-counting as described previously (3) and summarized below. When over-counting is present in a super-resolution image, the measured auto-correlation as a function of distance r, $g_{meas}(r)$, has the form

$$g_{meas}(r) = [\delta(r)/\rho + g(r>0)]*g_{PSF}(r),$$

where here the terms in square brackets are the delta function present at r = 0 ($\delta(r)$) plus the auto-correlation arising from the real distribution of labeled protein centers at distances greater than r = 0 ($g(r>0)$). Both terms are convoluted (*) with the correlation function of the effective point spread function (PSF) of the measurement $g_{PSF}(r)$, as described in detail in (3)). ρ is the average density of labeled molecules in the analyzed area. If a Gaussian shape of the PSF is assumed, the equation becomes

$$g_{meas}(r) = \exp\{-r^2/4\sigma^2\}/(4\pi\,\sigma^2\,\rho) + g(r>0) *g_{PSF}(r)$$

where the first term represents the contribution to $g_{meas}(r)$ of over-counting. g_{PSF} is estimated by comparing the auto-correlation of images reconstructed from all identified single molecule centers to those of images reconstructed from data grouped to account for localized single molecules within a threshold of twice the localization precision and are identified in sequential frames as described previously (3). g_{PSF} is then fit to a two-dimensional Gaussian function to determine σ, and we assume a surface density of the receptor to be 200 molecules/μm^2 (4). The measured correlation function is then fit to the above equation to determine the correlation function due to the real distribution of labeled molecules. $g(r>0)$ is approximated by an exponential function, $1+Aexp(-r/\xi)$, and A and ξ are extracted as fit parameters.

Cross-correlation functions from two-color experiments do not contain additional contributions from over-counting and can be fit to a single filtered exponential function to extract clustering parameters. Measured cross-correlations are of the form:

$$g_{meas}(r) = g_{PSF}(r)*g(r>0)$$

where $g(r>0)$ represents the correlation function arising from the real distribution of labeled molecules at distances greater than r = 0 and $g_{PSF}(r)$ is a function that applies a Gaussian filter with width proportional to the resolution of the image and represent the PSF of the measurement. $g(r>0)$ is well fit by a single exponential function, yielding

$$g_{Fit}(r) = g_{PSF}(r)*[1+ (Aexp(-r/\xi))]$$

where A and ξ are extracted as fit parameters.

Single particle tracking and diffusion analysis:

Single receptor trajectories are generated from fluorophore locations recorded within a masked area in live cell experiments using a simple tracking algorithm, in which localized probes in successive frames are linked in a trajectory if a localization in one frame falls within some maximum distance (here, 400-500nm) of a localization in the previous frame. This maximum step size is chosen by examining the resultant step size distribution and ensuring that it follows a log normal distribution. If a probe localization in one frame could be linked to more than one localization in the previous frame, i.e. the tracks merge, then the merged tracks are terminated to avoid artifacts. Also, if a point cannot be linked to the previous frame, the algorithm will look back up to several time points (3) to compensate for fast blinking of fluorophores or single molecules lost in image processing. Similar results were obtained with more complicated tracking algorithms that perform global minimizations (15).

Mean squared displacement (MSD) as a function of time interval τ is calculated over all trajectories that persist longer than two frames from the positions as a function of time (x(t) and y(t)). In general, the MSD in 2 dimensions is defined as

$$MSD(\tau) = \langle (x(t+\tau) - x(t))^2 \rangle + \langle y(t+\tau) - y(t))^2 \rangle$$

where the angled brackets denote an average over all t. MSD curves are tabulated for individual trajectories, or over all segments acquired in a single cell over a specified time window (typically 500 frames). Diffusion coefficients for individual molecules are only reported if trajectories extend at least some minimum number of frames (typically 14). Short and long time diffusion coefficients are determined through a weighted linear least squares fitting routine in Matlab (lscov), where weights were the inverse standard error of the mean for each MSD(τ).

In Figure 4D, we generate three dimensional histograms from single trajectory data by keeping track of the average diffusion coefficient (D_S) for single tracks, and the average density of receptors along each trajectory. The average density along the trajectory is determined by first reconstructing a super-resolution image from the first point of all trajectories localized within a 1000 frames (40 s) of acquired raw data. For Figure 4D, this image had a pixel dimension of 20nm by 20nm, and after reconstruction the image was convolved with a Gaussian filter with half-width of 40nm. This intensity image is then normalized so that the total average surface density is maintained at 200/μm^2. Finally, long trajectories were placed upon this image and the pixel value at each localized point along the trajectory was averaged. The three dimensional histogram was constructed by binning in both diffusion coefficient and average intensity. Histograms were filtered with a Gaussian function with half-width ≤1bin in order to smooth contours.

Ca^{2+} mobilization measurements:

RBL-2H3 cells were plated in 35mm dishes and allowed to adhere at 37 °C overnight. Cells were then sensitized with 1ug/ml unlabeled IgE for at least 2h at 37 °C prior to imaging. The cells were rinsed then labeled with the Ca^{2+}-sensitive dye Fluo-4-AM by incubating in 0.4µg of dye in 1ml of BSS containing 1mg/ml BSA (BSS-BSA) for 10min at room temperature. Cells were rinsed again to remove excess dye and imaged immediately in either BSS-BSA or in imaging buffer (IB) used for super-resolution experiments at room temperature. Fluo-4 fluorescence intensity was imaged at 2 fps under 10x

magnification. Samples were monitored as the cells were stimulated by addition of either 1 or 0.1 μM DNP-BSA 5 minutes after the start of imaging. To test the effects of cholesterol perturbation on cellular Ca^{2+} responses, MβCD or MβCD+chol was added to the dish 5 minutes after the start of imaging at a final concentration of 10mM and allowed to incubate for 5 minutes before cells were stimulated with 0.1 μM DNP-BSA as above. Fluo-4 intensity for each cell was determined by recording the average fluorescence intensity within a circle of radius 5 pixels (7.25μm) from the localized cell center as a function of time. The time averaged fractional intensity is normalized to 1 for each cell prior to treatments, and signals from at least 500 cells are averaged to obtain the average intensity traces shown in Figs. 3, 7, and S1. Small reductions in average Fluo-4 intensity vs. time due to bleaching and/or dye leakage were corrected for by fitting any downward slope present in the average Fluo-4 intensity curve within the first five minutes of imaging, prior to stimulation or addition of perturbation. The average intensity curve for all time points is then normalized by this fit. For cumulative curves of Ca^{2+} mobilization initiation events, individual cells are defined as having initiated a Ca^{2+} response if their intensity increases by a factor of 2.5 more than the average intensity of the cell prior to treatments.

Degranulation experiments:

To test the effects of imaging buffer on RBL degranulation, cells were sensitized with unlabeled anti-DNP IgE at a final concentration of 1μg/mL and plated at a density of 0.5 X 10^6 cells per well in a 96-well plate overnight at 37 °C. Adherent cells were washed in BSS-BSA and then washed into either BSS-BSA, live cell imaging buffer (IB) without a reducing agent or oxygen scavenging enzymes (135mM NaCl, 5mM KCl, 1mM $MgCl_2$, 1.8mM $CaCl_2$, 55mM glucose, 30mM Tris, at pH 8), or complete imaging buffer which includes reducing agents and oxygen scavenging enzymes (135mM NaCl, 5mM KCl, 1mM $MgCl_2$, 1.8mM $CaCl_2$, 55mM glucose, 30mM Tris, at pH 8 *with* 500μg/mL glucose-oxidase, 40μg/mL catalase, and 10, 50 or 100 mM glutathione or 10 mM β-mercaptoethanol at pH 8). After the addition of multivalent ligand DNP_{24}-BSA at 1ug/ml final concentration , the cells were incubated at 37°C for an hour, and the supernatants were taken from each well to assay the extent of β -hexosaminidase release from the cells as previously described (1). Stimulated degranulation is expressed as a percentage of the total cellular β-hexosaminidase activity present in cell lysates after solubilization in 0.1% Triton X-100.

To test the effects of cholesterol perturbations on RBL-2H3 degranulation, cells were plated and sensitized with unlabeled IgE in the same manner as above. After washing with BSS-BSA, cells were washed into BSS-BSA, complete IB, or complete IB containing 10mM MβCD or MβCD+chol. Following a 5 min incubation, DNP-BSA was added to some samples at .1ug/ml final concentration and the samples were incubated at 37°C for one hour. β-hexosaminidase released was assayed as above.

SUPPORTING REFERENCES

1. Naal, R.M.Z.G., J. Tabb, D. Holowka, and B. Baird. 2004. In situ measurement of degranulation as a biosensor based on RBL-2H3 mast cells. Biosens. Bioelectron. 20: 791–796.

2. Veatch, S.L., E.N. Chiang, P. Sengupta, D.A. Holowka, and B.A. Baird. 2012. Quantitative nanoscale analysis of IgE-FcεRI clustering and coupling to early signaling proteins. J. Phys. Chem. B. 116: 6923–6935.

3. Veatch, S.L., B.B. Machta, S.A. Shelby, E.N. Chiang, D.A. Holowka, et al. 2012. Correlation functions quantify super-resolution images and estimate apparent clustering due to over-counting. PloS One. 7: e31457.

4. Erickson, J., B. Goldstein, D. Holowka, and B. Baird. 1987. The effect of receptor density on the forward rate constant for binding of ligands to cell surface receptors. Biophys. J. 52: 657–662.

5. Machta, B.B., S. Papanikolaou, J.P. Sethna, and S.L. Veatch. 2011. Minimal Model of Plasma Membrane Heterogeneity Requires Coupling Cortical Actin to Criticality. Biophys. J. 100: 1668–1677.

6. Andrews, N.L., K.A. Lidke, J.R. Pfeiffer, A.R. Burns, B.S. Wilson, et al. 2008. Actin restricts FcεRI diffusion and facilitates antigen-induced receptor immobilisation. Nat. Cell Biol. 10: 955–963.

7. Sheets, E.D., D. Holowka, and B. Baird. 1999. Critical Role for Cholesterol in Lyn-mediated Tyrosine Phosphorylation of FcεRI and Their Association with Detergent-resistant Membranes. J. Cell Biol. 145: 877–887.

8. Surviladze, Z., L. Dráberová, M. Kovářová, M. Boubelík, and P. Dráber. 2001. Differential sensitivity to acute cholesterol lowering of activation mediated via the high-affinity IgE receptor and Thy-1 glycoprotein. Eur. J. Immunol. 31: 1–10.

9. Yamashita, T., T. Yamaguchi, K. Murakami, and S. Nagasawa. 2001. Detergent-resistant membrane domains are required for mast cell activation but dispensable for tyrosine phosphorylation upon aggregation of the high affinity receptor for IgE. J. Biochem. (Tokyo). 129: 861–868.

10. Kato, N., M. Nakanishi, and N. Hirashima. 2003. Cholesterol depletion inhibits store-operated calcium currents and exocytotic membrane fusion in RBL-2H3 cells. Biochemistry (Mosc.). 42: 11808–11814.

11. Silveira e Souza, A.M.M., V.M. Mazucato, R.O. de Castro, F. Matioli, P. Ciancaglini, et al. 2008. The α-galactosyl derivatives of ganglioside GD1b are essential for the organization of lipid rafts in RBL-2H3 mast cells. Exp. Cell Res. 314: 2515–2528.

12. Gosse, J.A., A. Wagenknecht-Wiesner, D. Holowka, and B. Baird. 2005. Transmembrane Sequences Are Determinants of Immunoreceptor Signaling. J. Immunol. 175: 2123 –2131.

13. Larson, D.R., J.A. Gosse, D.A. Holowka, B.A. Baird, and W.W. Webb. 2005. Temporally resolved interactions between antigen-stimulated IgE receptors and Lyn kinase on living cells. J. Cell Biol. 171: 527–536.

14. Hardy, R.R. 1986. Handbook of Experimental Immunology. 4th ed. Oxford, UK: Blackwell Scientific Publication.

15. Jaqaman, K., D. Loerke, M. Mettlen, H. Kuwata, S. Grinstein, et al. 2008. Robust single-particle tracking in live-cell time-lapse sequences. Nat. Methods. 5: 695–702.